JOURNAL OF Materials CHEMISTRY

Crystal chemistry and physical properties of complex lithium spinels $Li_2MM'_3O_8$ (M = Mg, Co, Ni, Zn; M′ = Ti, Ge)

Hiroo Kawai,[a] Mitsuharu Tabuchi,[b] Mikito Nagata,[c] Hisashi Tukamoto[c] and Anthony R. West[a]

[a]*Department of Chemistry, University of Aberdeen, Meston Walk, Aberdeen, Scotland, UK AB24 3UE*

[b]*Osaka National Research Institute, 1-8-31 Midorigaoka, Ikeda, Osaka 563, Japan*

[c]*Corporate R&D Centre, Japan Storage Battery Company Limited, Nishinosho, Kisshoin, Minami-ku, Kyoto 601, Japan*

The spinels $Li_2MM'_3O_8$ (MM′ = MgTi, CoTi, CoGe, NiGe and ZnGe) are cubic with space group $P4_332$. Simple crystal field theory qualitatively explains the distribution of M over tetrahedral and octahedral sites: Ni occupies only octahedral sites, whereas Zn, Mg and Co show strong preference for tetrahedral sites. 1 : 3 cation ordering of Li/M and M′ occurs on the octahedral sites. The titanates undergo an order–disorder phase transition involving the octahedral cations at high temperatures, whereas the ordered phase is maintained until melting for the germanates. Solid solutions $Li_{2-2X}M_{1+3X}M'_{3-X}O_8$ form at both sides of the $Li_2MM'_3O_8$ stoichiometry for the titanates; but there is no substantial range of solid solution for $Li_2ZnGe_3O_8$ and $Li_2NiGe_3O_8$. The occurrence of order–disorder phenomena and solid solutions in the titanates is attributed to the similarity in size of Li, M and Ti, whereas the smaller Ge is less able to disorder with Li/M. M is shown to be divalent from magnetic susceptibility measurements (for Co and Ni) with the support of conductivity data. The samples containing Co and Ni are paramagnetic down to 5 K. From impedance measurements on pellets with blocking electrodes, the main conductive species is deduced to be Li^+: the activation energies for conduction are high, $0.55 < \Delta H/eV < 2.14$. Cyclic voltammograms show a set of reversible peaks at *ca.* 1.5 V *vs.* Li/Li^+ for the titanates, attributed to the $Ti^{3+/4+}$ couple, but no Li could be electrochemically extracted from either titanates or germanates up to 5 V *vs.* Li/Li^+.

The ideal spinel structure consists of a cubic close-packed array of anions, with one eighth of the tetrahedral and one half of the octahedral interstices occupied by cations, having the general formula $A[B_2]X_4$, where A is a tetrahedrally surrounded cation, B an octahedrally surrounded one, and X an anion. The crystal chemistry of binary spinel oxides such as $M^{2+}M^{3+}{}_2O_4$ and $M^{4+}M^{2+}{}_2O_4$ has been studied in detail.[1–4] The cation distributions were only partially explained on the basis of ionic bonding and were affected as well by the individual site preference of cations.[1–4] In contrast to binary spinel oxides, the crystal chemistry of ternary spinel oxides is less well understood.

A considerable number of ternary lithium spinels with the composition $Li_2MM'_3O_8$ has been synthesised.[5–12] Blasse[9] determined approximate cation distributions for several of these: no systematic correlation with the individual site preference of cations was obtained, but the cation distributions were partially accounted for by introducing an anion polarisation effect, in addition to the electrostatic energy term.

Complex spinel phases allow either tetrahedral or octahedral sites to be occupied by more than one kind of cation. The distributions over both sets of interstices tend to be random at high temperatures, while they are often ordered at low temperatures with lowering of the symmetry. 1 : 3 cation ordering in octahedral sites is commonly observed at the composition $Li_2MM'_3O_8$.[5–11] In $Li_2ZnTi_3O_8$, for instance, Li and Ti show 1 : 3 cation ordering over two sets of octahedral sites below 1150 °C at which temperature an order–disorder phase transition occurs.[13]

The composition $Li_2MM'_3O_8$ may be considered as a spinel composition on the line between the two binary compositions $Li_4M^{4+}{}_5O_{12}$ and $M^{2+}{}_2M^{4+}O_4$; the cation to anion ratio remains at 3 : 4 throughout, but 1 : 3 cation order is possible at this composition. A complete range of spinel-like solid solution, $Li_{2-2X}Zn_{1+3X}Ti_{3-X}O_8$: $-1/3 \leqslant X \leqslant 1$ has been recently reported on the line $Li_4Ti_5O_{12}$–Zn_2TiO_4: these show 1 : 3 cation order for a small range of compositions close to $Li_2ZnTi_3O_8$, but are disordered to either side.[13]

In order to better understand the crystal chemistry and properties of this series of spinels, it is necessary to examine the distribution, valence state, and ordering of cations more accurately and to survey the formation of solid solutions for lithium spinels $Li_2MM'_3O_8$. In this paper, we focus on the compositions $Li_2MM'_3O_8$ (M = Mg, Co, Ni, Zn; M′ = Ti, Ge), and discuss (1) the cation distributions, (2) valence states of transition-metal ions, (3) order–disorder phase transitions, (4) formation of solid solutions, and (5) magnetic, electrical and electrochemical properties.

Experimental

Starting materials were Li_2CO_3, MgO, CoO, NiO, ZnO, TiO_2 and GeO_2, all reagent grade. Stoichiometric amounts of the dried reagents were mixed in an agate mortar, using acetone to form a paste, dried and fired in air, initially at 650 °C for a few hours to decarbonate and then at 800 °C for 12 h. The calcined powders were reground, pelleted and reacted between 900 and 950 °C for 12 h to 3 days, depending upon starting material and composition. The products were quenched in air from the reaction temperatures.

Samples were initially examined for completeness of reaction and phase purity by powder X-ray diffraction (XRD) with a Philips Hagg Guinier focusing camera, Cu-Kα_1 radiation. For lattice parameter determination and Rietveld refinement, data were collected with a Stoe Stadi/P diffractometer in transmission mode using a small linear position sensitive detector of resolution 0.02°, Cu-Kα_1 radiation. A scan range of $8 < 2\theta/° < 113$ in steps of 0.2° was used for Rietveld refinement. The data analysis was carried out with the Stoe software

package: lattice parameter refinement was performed using LATREF, and Rietveld refinement using the pattern fitting structure refinement (PFSR) program. Powder neutron diffraction data were collected for $Li_2ZnGe_3O_8$ on the Polaris medium resolution diffractometer at the UK spallation neutron source ISIS, Rutherford Appleton Laboratory. The crystal data, collected over the time-of-flight range 2.300–19.570 μs, in the highest resolution, backscattering detectors were refined by the Rietveld method with the program TF14LS.

For conductivity measurements, pellets (8 mm diameter; 2–3 mm thickness) were cold-pressed uniaxially at 150 MPa and sintered at 950 °C for 24 h, in order to increase their mechanical strength. Gold paste electrodes were coated onto opposite sides of the sintered pellets which were gradually heated to 800 °C to decompose the paste and harden the Au residue. Impedance measurements between 30 mHz and 1 MHz, used combined Solartron 1250/1286 and Hewlett-Packard 4192 instrumentation. The data were analysed in three formalisms, the complex impedance (Z^*), admittance (Y^*), and modulus (M^*),[14] using in-house software.

Thermal analysis in air, heating/cooling rates of 10 °C min^{-1}, used a Stanton Redcroft STA1500 simultaneous TG/DTA instrument with alumina as an inert reference for differential thermal analysis, DTA. Magnetic measurements were performed under He from room temperature to 5 K, using a MB-3 Shimazu Faraday balance and Quantum Design MPMS2 SQUID magnetometer. The standard used for magnetic susceptibility calibration was Tutton's salt, $(NH_4)_2Mn(SO_4)_2 \cdot 6H_2O$.

Cyclic voltammograms were made over the potential range 1–5 V *vs.* Li/Li^+ with scan speed 0.1 mV s^{-1}, using a Hokuto-Denco HA151 potentiostat galvanostat linked to a Hokuto-Denco HB111 function generator. A three-electrode cell was used. The working electrode consisted of $Li_2MM'_3O_8$, mixed with 5 mass% acetylene black (active material) and 8 mass% binder made of poly(vinylidene fluoride) and *N*-methyl-2-pyrrolidone. The counter and reference electrodes consisted of a strip of Li metal foil. The electrolyte was 1 M $LiPF_6$ dissolved in either propylene carbonate or 50/50 vol.% mixture of ethylene carbonate and diethyl carbonate.

Melting temperatures were determined approximately from the appearance of samples after each stage of a stepwise heating cycle. The possible formation of solid solutions $Li_{2-2X}M_{1+3X}M'_{3-X}O_8$ was checked at either side of the $Li_2MM'_3O_8$ stoichiometry ($X=0$), for compositions $X=0.11$ and -0.067.

Results and Discussion

Phase-pure spinels were obtained at the following compositions: $Li_2MgTi_3O_8$, $Li_2CoTi_3O_8$, $Li_2CoGe_3O_8$, $Li_2NiGe_3O_8$ and $Li_2ZnGe_3O_8$, and had the colours shown in Table 1. Their powder XRD patterns were indexed in the cubic space group $P4_332$ with lattice parameters, $\approx 8.18 < a/Å < \approx 8.38$, Table 2. The titanates had larger lattice parameters than the corresponding germanates, consistent with the larger size of Ti^{4+} compared with Ge^{4+}.[15] $Li_2MgGe_3O_8$ and $Li_2NiTi_3O_8$ showed complicated XRD patterns which could not be indexed as single phase spinels; further work on them is in progress. $Li_2ZnTi_3O_8$ was not prepared; data for it[13] are listed in Tables 1 and 2.

Structure refinement

Structure refinement using the Rietveld method has been recently carried out by Ohtsuka's group[16,17] for the spinel phases obtained in this study. The refinement was repeated on our diffraction data, using more extensive structure models within the space group $P4_332$. The starting atomic positions were those given in ref. 16 and 17. The value of 0.05 was used as the initial isotropic thermal parameters (U_{iso}) of all the atomic positions. The total occupancy of 8c, 4b and 12d cation sites was fixed at unity; oxygens were situated at 8c and 24e sites with full occupancy. The effect of varying the cation distributions on 8c, 4b and 12d sites was examined initially by generating theoretical powder XRD patterns, using the starting atomic coordinates and thermal parameters, with the program THEO in the Stoe software package. Rietveld refinement was then carried out for several likely models, to examine detailed occupancy of cation sites.

Profile parameters were initially allowed to refine. After

Table 1 Physical data for spinel phases $Li_2MM'_3O_8$

composition	colour	melting points /°C	DTA peaks[a,b] /°C	formation of s.s.[c] $X=0.11$	formation of s.s.[c] $X=-0.067$
$Li_2ZnTi_3O_8$	white	1410[d]	1165[d,e]	yes[d]	yes[d]
$Li_2ZnGe_3O_8$	white	1000	none	no	no
$Li_2MgTi_3O_8$	white	1410	990[e]	yes	yes
$Li_2CoTi_3O_8$	green	1250	907[e]	yes	yes
$Li_2CoGe_3O_8$	purplish blue	980	none	yes	no
$Li_2NiGe_3O_8$	greenish sky	970	none	no	no

[a]DTA peak temperatures on the heating cycle. Peak temperatures on cooling were 15–35 °C lower. [b]Observed from room temperature to *ca.* 50 °C below the melting points for the germanates, and at least up to *ca.* 1200 °C for the titanates. [c]s.s. denotes the solid solution $Li_{2-2X}M_{1+3X}M'_{3-X}O_8$. [d]After Hernandez *et al.*, ref. 13. [e]Sharp peak.

Table 2 Structural data for spinel phases $Li_2MM'_3O_8$

composition	symmetry (space group)	lattice parameter a/Å	cation distributions[a]	Y[b]	octahedral-site preference energy for M^{2+}[c]/kcal mol^{-1}
$Li_2ZnTi_3O_8$	cubic[d] ($P4_332$[d])	8.3710(2)[d]	$Li_{0.5}Zn_{0.5}[(Li_{0.5})Ti_{1.5}]$[d]	0.5	0 (Zn^{2+})
$Li_2ZnGe_3O_8$	cubic ($P4_332$)	8.1961(5)	$Li_{0.5}Zn_{0.5}[(Li_{0.5})Ge_{1.5}]$	0.5	0 (Zn^{2+})
$Li_2MgTi_3O_8$	cubic ($P4_332$)	8.3774(9)	$Li_{0.55}Mg_{0.45}[(Li_{0.45}Mg_{0.05})Ti_{1.5}]$	0.45	
$Li_2CoTi_3O_8$	cubic ($P4_332$)	8.3766(12)	$Li_{0.55}Co_{0\cdot45}[(Li_{0.45}Co_{0.05})Ti_{1.5}]$	0.45	2.1 (Co^{2+})
$Li_2CoGe_3O_8$	cubic ($P4_332$)	8.2098(4)	$Li_{0.55}Co_{0.45}[(Li_{0.45}Co_{0.05})Ge_{1.5}]$	0.45	2.1 (Co^{2+})
$Li_2CuTi_3O_8$	cubic[e]	8.39[e]		0.3[e]	15.6 (Cu^{2+})
$Li_2NiGe_3O_8$	cubic ($P4_332$)	8.1799(2)	$Li[(Ni_{0.5})Ge_{1.5}]$	0	22.8 (Ni^{2+})

[a]In $A[(B_{0.5})B'_{1.5}]O_4$, A denotes tetrahedral 8c sites, B octahedral 4b sites, and B′ octahedral 12d sites. [b]Y changes in the formula $Li_{1-Y}M_Y[(Li_YM_{0.5-Y})M'_{1.5}]O_4$, $0 \leqslant Y \leqslant 0.5$. [c]After McClure, ref. 2. [d]After Hernandez *et al.*, ref. 13. [e]After Blasse, ref. 6. $Y=0.3$ for $Li_2CuTi_3O_8$ has been recently confirmed by the Rietveld method.[19]

convergence, the atomic positions were refined in the order: heavy atoms (M and M′), oxygen, and lithium; isotropic thermal vibration parameters were then refined in the same order. In some cases, isotropic thermal parameters for oxygen and sites containing high concentrations of lithium would not converge or became negative during refinement. These thermal parameters were then fixed at 0.05. When the model allowed more than one kind of cation to occupy the same sites, their positions were refined with the same atomic coordinates and thermal parameters. Of the various models tested, the model with minimum R values[18] was used for the final stage of refinement. At this stage, thermal parameters were fixed at the refined values, and atomic positions and occupancy of cation sites were allowed to refine, but with the total occupancy fixed at unity and the composition fixed at $Li_2MM'_3O_8$. In situations where the occupancy of cation sites was modified, atomic positions and temperature parameters were refined again, with the occupancy fixed at the modified values. Therefore, the final parameter listings do not have estimated error data for the occupancies, but list estimated error values for the thermal parameters. The final structure refinement parameters are given in Tables 3–7, with R values and bond lengths. The refined cation distributions are listed in Table 2. The final profile fit is shown in Fig. 1 for $Li_2MgTi_3O_8$ as an example. The final R_P and R_{WP} values for $Li_2NiGe_3O_8$ were considerably greater than those of the other phases. This is attributed to the inadequate profile fit probably caused by difficulty in describing the peak shape, owing to a possible interaction between Ni and Cu-Kα_1 radiation.

For $Li_2ZnGe_3O_8$, Rietveld refinement was additionally carried out using powder neutron diffraction data, following the same refinement procedure; the structure refined to the same cation distribution and similar atomic coordinates to the one obtained using powder XRD data, thus supporting the validity of refinement results using our powder XRD data. Structure refinement parameters from neutron data are given for $Li_2ZnGe_3O_8$ in Table 7. It is seen clearly from the comparison of the estimated error values for atomic positions and thermal parameters that neutron data offer more precise refinement results than XRD data.

Structure descriptions and cation distributions

The refined atomic positions are in good agreement with those reported previously.[16,17] The cation distributions may be expressed by the formula, $Li_{1-Y}M_Y[(Li_YM_{0.5-Y})M'_{1.5}]O_4$ ($0 \leqslant Y \leqslant 0.5$). Li and M are distributed over tetrahedral 8c and octahedral 4b sites according to Y. Y therefore denotes the degree of cation mixing in tetrahedral sites. The refinements revealed that M′, *i.e.*, Ti and Ge are situated only in octahedral 12d sites. For $Li_2NiGe_3O_8$, $Y=0$; tetrahedral sites are occupied only by Li; Ni and Ge are located in octahedral sites with 1:3 order, Fig. 2. For $Li_2MgTi_3O_8$, $Li_2CoTi_3O_8$ and $Li_2CoGe_3O_8$, the previous refinements[16,17] concluded that $Y=0.5$, but our refinements showed minimum R values when $Y=0.45$; Li and M are randomly distributed in tetrahedral sites, whereas Li/M and M′ show 1:3 order in octahedral sites. For $Li_2ZnGe_3O_8$, $Y=0.5$; there is complete 1:3 order of Li and Ge in octahedral sites; Li and Zn are distributed randomly in tetrahedral sites.

Bond lengths calculated were appropriate for spinel oxides, supporting the structure model refined. In situations where low-scattering Li fully occupies tetrahedral 8c sites, *i.e.*, $Li_2NiGe_3O_8$, $Y=0$, the 8c atomic coordinates and the corresponding Li—O bond lengths should be viewed with care, however, Table 6.

Table 3 Structure refinement parameters and bond lengths for $Li_2MgTi_3O_8$ from X-ray data. Space group $P4_332$; $a=8.3774(9)$ Å; $R_P=2.41\%$; $R_{WP}=3.26\%$

atom	site	x/a	y/b	z/c	U_{iso}	occupancy
Li(1)	8c	0.998(2)	0.998(2)	0.998(2)	0.027(3)	0.55
Mg(1)	8c	0.998(2)	0.998(2)	0.998(2)	0.027(3)	0.45
Li(2)	4b	0.625	0.625	0.625	0.025(15)	0.9
Mg(2)	4b	0.625	0.625	0.625	0.025(15)	0.1
Ti	12d	0.125	0.3687(5)	0.8812(5)	0.023(1)	1
O(1)	8c	0.391(2)	0.391(2)	0.391(2)	0.013(7)	1
O(2)	24e	0.107(2)	0.129(1)	0.390(1)	0.021(3)	1

	distance to O(1)/Å	distance to O(2)/Å	average distance to oxygen/Å
Li(1)/Mg(1)	2.02(2)	1.97(2) (×3)	1.98
Li(2)/Mg(2)		2.14(1) (×6)	2.14
Ti	2.02(2) (×2)	1.90(1) (×2)	1.97
		1.98(2) (×2)	

Table 4 Structure refinement parameters and bond lengths for $Li_2CoTi_3O_8$ from X-ray data. Space group $P4_332$; $a=8.3766(12)$ Å; $R_P=2.30\%$; $R_{WP}=3.05\%$

atom	site	x/a	y/b	z/c	U_{iso}	occupancy
Li(1)	8c	0.001(4)	0.001(4)	0.001(4)	0.013(6)	0.55
Co(1)	8c	0.001(4)	0.001(4)	0.001(4)	0.013(6)	0.45
Li(2)	4b	0.625	0.625	0.625	0.06(6)	0.9
Co(2)	4b	0.625	0.625	0.625	0.06(6)	0.1
Ti	12d	0.125	0.368(2)	0.882(2)	0.020(4)	1
O(1)	8c	0.375(7)	0.375(7)	0.375(7)	0.05	1
O(2)	24e	0.100(8)	0.127(4)	0.387(5)	0.05	1

	distance to O(1)/Å	distance to O(2)/Å	average distance to oxygen/Å
Li(1)/Co(1)	1.83(7)	1.98(6) (×3)	1.94
Li(2)/Co(2)		2.12(5) (×6)	2.12
Ti	2.15(6) (×2)	1.83(4) (×2)	2.00
		2.01(7) (×2)	

Table 5 Structure refinement parameters and bond lengths for $Li_2CoGe_3O_8$ from X-ray data. Space group $P4_332$; $a=8.2098(4)$ Å; $R_P=1.88\%$; $R_{WP}=2.46\%$

atom	site	x/a	y/b	z/c	U_{iso}	occupancy
Li(1)	8c	0.005(1)	0.005(1)	0.005(1)	0.027(3)	0.55
Co(1)	8c	0.005(1)	0.005(1)	0.005(1)	0.027(3)	0.45
Li(2)	4b	0.625	0.625	0.625	0.05	0.9
Co(2)	4b	0.625	0.625	0.625	0.05	0.1
Ge	12d	0.125	0.3759(6)	0.8742(6)	0.016(1)	1
O(1)	8c	0.382(6)	0.382(6)	0.382(6)	0.03(1)	1
O(2)	24e	0.096(7)	0.123(1)	0.395(2)	0.015(8)	1

	distance to O(1)/Å	distance to O(2)/Å	average distance to oxygen/Å
Li(1)/Co(1)	1.95(5)	2.00(4) (×3)	1.99
Li(2)/Co(2)		2.06(3) (×6)	2.06
Ge	1.99(5) (×2)	1.83(1) (×2)	1.91
		1.90(6) (×2)	

Table 6 Structure refinement parameters and bond lengths for $Li_2NiGe_3O_8$ from X-ray data. Space group $P4_332$; $a=8.1799(2)$ Å; $R_P=8.03\%$; $R_{WP}=12.14\%$

atom	site	x/a	y/b	z/c	U_{iso}	occupancy
Li	8c	0.018(8)	0.018(8)	0.018(8)	0.05	1
Ni	4b	0.625	0.625	0.625	0.012(4)	1
Ge	12d	0.125	0.3777(7)	0.8723(7)	0.013(1)	1
O(1)	8c	0.385(3)	0.385(3)	0.385(3)	0.01(1)	1
O(2)	24e	0.094(3)	0.127(2)	0.394(2)	0.012(5)	1

	distance to O(1)/Å	distance to O(2)/Å	average distance to oxygen/Å
Li	2.17(7)	1.94(7) (×3)	2.00
Ni		2.08(2) (×6)	2.08
Ge	1.95(3) (×2)	1.82(2) (×2)	1.89
		1.90(2) (×2)	

Table 7 Structure refinement parameters and bond lengths for $Li_2ZnGe_3O_8$ from neutron data. Space group $P4_332$; $a=8.1961(5)$ Å; $R_P=2.49\%$; $R_{WP}=2.10\%$

atom	site	x/a	y/b	z/c	B_{iso}	occupancy
Li(1)	8c	0.00488(14)	0.00488(14)	0.00488(14)	0.203(12)	0.5
Zn	8c	0.00488(14)	0.00488(14)	0.00488(14)	0.203(12)	0.5
Li(2)	4b	0.625	0.625	0.625	0.96(3)	1
Ge	12d	0.125	0.37464(4)	0.87536(4)	0.226(3)	1
O(1)	8c	0.38653(4)	0.38653(4)	0.38653(4)	0.302(8)	1
O(2)	24e	0.09906(4)	0.13104(5)	0.39490(4)	0.321(4)	1

	distance to O(1)/Å	distance to O(2)/Å	average distance to oxygen/Å
Li(1)/Zn	2.008(1)	1.953(1) (×3)	1.967
Li(2)		2.1156(3) (×6)	2.1156
Ge	1.9619(4) (×2)	1.8416(5) (×2)	1.9008
		1.8989(3) (×2)	

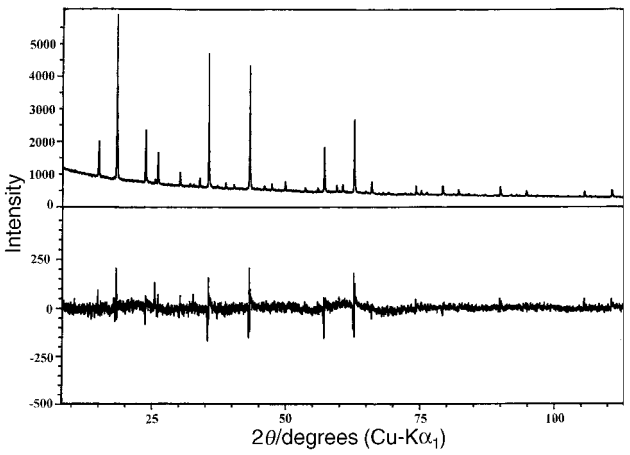

Fig. 1 Observed and difference powder XRD profiles for $Li_2MgTi_3O_8$

As shown in the following sections, magnetic susceptibility and conductivity data demonstrated that M is divalent for all the spinel phases obtained, *i.e.*, the formulae are $Li_2M^{2+}M'^{4+}{}_3O_8$. Li and M have similar ionic radii[15] and differ in oxidation state only by unity. The electrostatic energies, *i.e.*, the sum of the Coulomb and Born repulsion energies, are thus expected to be similar throughout the range $0 \leqslant Y \leqslant 0.5$ in any one phase. The difference in Y between the spinel phases is then attributable mainly to either the difference in individual site preference of M or oxygen polarisation. McClure[2] and simultaneously, Dunitz and Orgel[3] calculated site preference energies of transition-metal ions using crystal field theory; the difference between the energy values for octahedral and tetrahedral stabilisation was used as a measure of the octahedral-site preference. It is seen from Table 2 that Y, *i.e.*, the concentration of M in tetrahedral 8c sites decreases roughly with increasing octahedral-site preference energy of M, consistent with the expectations from crystal field theory. Zn^{2+} is usually regarded as forming covalent bonds in tetrahedral

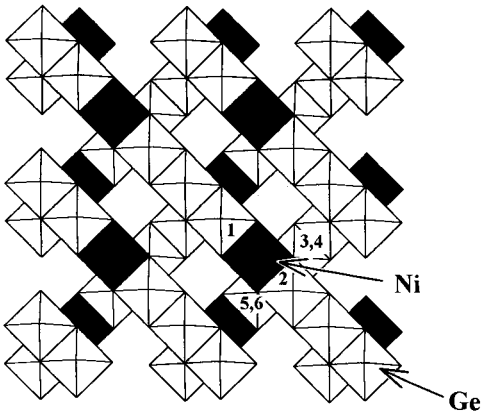

Fig. 2 Projection of the spinel structure of $Li_2NiGe_3O_8$ showing the 4b (shaded NiO_6) and 12d (unshaded GeO_6) octahedra. Each NiO_6 shares edges with six GeO_6: for the Ni octahedron indicated, four GeO_6 octahedra: 1, 2, 3 and 5, are shown; the other two, 4 and 6, are above the plane of the projection.

coordination,[20] consistent with $Y=0.5$ for $Li_2ZnTi_3O_8$ and $Li_2ZnGe_3O_8$.

Order–disorder phenomena and solid solution formation

After reaction to give single phase products, all samples were annealed at 800 °C, then cooled stepwise to 300 °C in intervals of 100 °C, with at least 12 h at each temperature. There were no phase changes such as decomposition or additional ordering induced by the annealing. The spinel phases with 1:3 cation ordering are thus thermodynamically stable at low temperatures.

For all the titanates, DTA traces showed a set of reversible peaks on heating and cooling, Table 1. Exotherms on cooling were 15–35 °C lower than the corresponding endotherms on heating, attributable to thermal hysteresis. Sharp peaks were observed which imply a first-order phase transition. There were no mass changes through the peaks, at least up to *ca.* 1200 °C, Table 1. The thermal anomalies are probably due to an order–disorder phase transition involving cations in the octahedral sites, as shown previously for $Li_2ZnTi_3O_8$.[13] The high-temperature disordered phases were, however, not retained by air quenching from above the peak temperatures; instead, the low-temperature ordered phases formed. No DTA peaks or mass changes were detectable for any of the germanates, Table 1. The ordered phases were thus maintained until melting temperatures, without undergoing any phase transitions.

For the two titanates, a solid solution $Li_{2-2X}M_{1+3X}M'_{3-X}O_8$ formed on both sides of the $Li_2MM'_3O_8$ stoichiometry ($X=0$) as shown for two compositions, $X=0.11$ and -0.067, Table 1. By contrast, with one exception there was no evidence of solid solution formation on either side of $X=0$ for the germanates. For $Li_2ZnGe_3O_8$, the composition $X=0.11$ gave a mixture of $Li_2ZnGe_3O_8$ and Zn_2GeO_4 (phenacite), and the composition $X=-0.067$ a mixture of $Li_2ZnGe_3O_8$ and an unidentified phase(s). For $Li_2NiGe_3O_8$, the composition $X=-0.067$ was a mixture of $Li_2NiGe_3O_8$ and $Li_4Ge_5O_{12}$; composition $X=0.11$ gave two spinels, $Li_2NiGe_3O_8$ and Ni_2GeO_4. $Li_2CoGe_3O_8$ was the only exception, having a range of solid solution towards Co_2GeO_4; composition $X=-0.067$ gave a mixture of $Li_2CoGe_3O_8$ and $Li_4Ge_5O_{12}$.

The general absence of both order–disorder transitions and solid solution formation in the germanates, but their presence in the titanates, probably has a common origin in the relative sizes of cations and in particular, in the small size of Ge^{4+}, in octahedral sites, compared with Ti^{4+}, Li^+ and M^{2+}. The Ge—O distances (12d sites) are all around 1.90 Å, significantly smaller than both Li/M—O distances (4b sites), average 2.10 Å and Ti—O distances (12d sites), average 1.99 Å. Thus, these size differences make less likely the disordering of Ge and Li/M over the octahedral sites. By contrast, the small difference in size of the Ti and Li/M sites makes disordering easier. The disorder can be introduced, either by raising the temperature or by varying the composition by means of the solid solution mechanism, $3M=2Li+M'$.

As listed in Table 1, all the titanates have melting temperatures higher than the germanates. The melting temperatures for the germanates are similar to the order–disorder phase transition temperatures for the titanates, in the temperature range 900–1000 °C.

Magnetic properties

Magnetic properties were examined for the samples containing Co and Ni. For all the samples, inverse molar susceptibility, χ_m^{-1}, changes linearly with temperature in the range 5–293 K, according to the Curie–Weiss law, $\chi_m^{-1}=(T-\theta)/C$, where θ is the Weiss constant, and C is a constant, Fig. 3. Even at 5 K, magnetizations, M, are small, and increase linearly with increasing applied field, H, without showing any evidence of spontaneous magnetization, Fig. 4. $Li_2CoTi_3O_8$, $Li_2CoGe_3O_8$ and $Li_2NiGe_3O_8$ are therefore paramagnetic down to 5 K.

Effective magnetic moments per Co or Ni, μ_{eff}, estimated from the susceptibility data, Fig. 3, are listed in Table 8. μ_{eff} for $Li_2CoTi_3O_8$ and $Li_2CoGe_3O_8$ are comparable to that of the spinel $Co[Rh_2]O_4$ in which the only paramagnetic ion, Co^{2+}, is located in tetrahedral sites: $\mu_{eff}/\mu_B=4.55$ for $Co[Rh_2]O_4$.[21] $Li_2NiGe_3O_8$ possesses μ_{eff} similar to that of the spinel $Ge[Ni_2]O_4$ which has the only paramagnetic ion, Ni^{2+}, in octahedral sites: $\mu_{eff}/\mu_B=3.24$ for $Ge[Ni_2]O_4$.[22] Co and Ni are thus likely to be divalent in $Li_2CoTi_3O_8$, $Li_2CoGe_3O_8$ and $Li_2NiGe_3O_8$.

In a spinel $A[B_2]X_4$, three types of magnetic interactions between paramagnetic ions should be taken into consideration, *i.e.*, A–A, A–B and B–B interactions. For $Li_2CoTi_3O_8$, $Li_2CoGe_3O_8$ and $Li_2NiGe_3O_8$, every 4b octahedron occupied by paramagnetic Co^{2+} or Ni^{2+} is surrounded by six 12d octahedra containing diamagnetic Ti^{4+} or Ge^{4+}, as a consequence of 1:3 cation ordering, Fig. 2. No B–B interactions between Co^{2+} or Ni^{2+} therefore occur in these ordered spinels. Tetrahedral A sites are occupied only by diamagnetic Li^+ in $Li_2NiGe_3O_8$. Neither A–A nor A–B interactions between Ni^{2+}

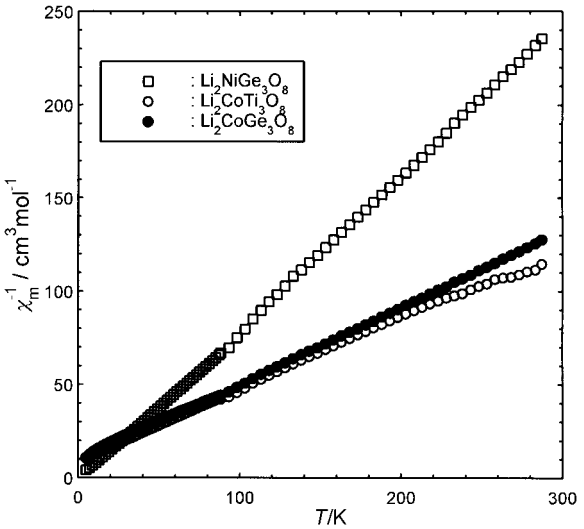

Fig. 3 Magnetic susceptibility data for spinel phases $Li_2MM'_3O_8$ in the temperature range 5–293 K

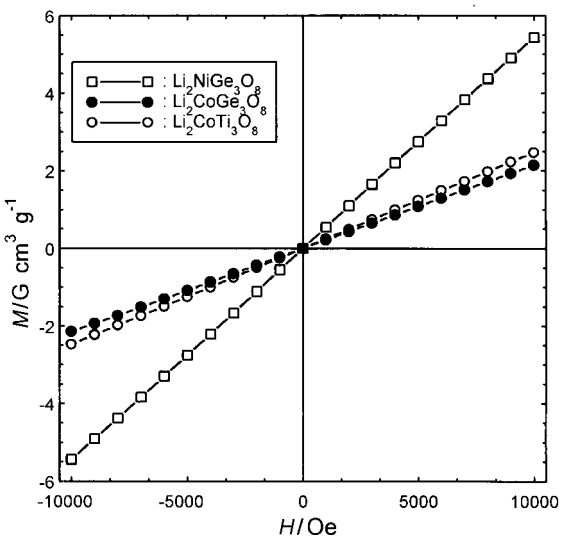

Fig. 4 Field dependence of magnetization for spinel phases $Li_2MM'_3O_8$ at 5 K

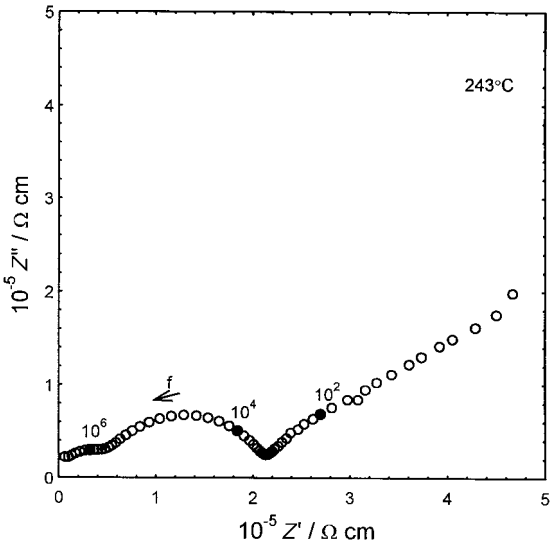

Fig. 5 Impedance data for $Li_2NiGe_3O_8$ at 243 °C

Table 8 Magnetic data for spinel phases $Li_2MM'_3O_8$

composition	μ_{eff}/μ_B[a]	θ/K	remarks
$Li_2CoTi_3O_8$	4.70(3)	−35(4)	paramagnetic down to 5 K
$Li_2CoGe_3O_8$	4.40(1)	−20(1)	paramagnetic down to 5 K
$Li_2NiGe_3O_8$	3.09(1)	7(1)	paramagnetic down to 5 K

[a]μ_B denotes the Bohr magneton.

thus take place in it. Ni^{2+} are then regarded as free ions without any magnetic interactions. This accounts for the very small θ value for $Li_2NiGe_3O_8$, Table 8. $Li_2CoTi_3O_8$ and $Li_2CoGe_3O_8$ have significantly negative θ values, Table 8. A–B interactions between Co^{2+} are expected to be negative. However, the concentration of Co^{2+} in the octahedral B sites is very small and appears to be inadequate to cause even short-range A–B interactions between Co^{2+}. Negative A–A interactions between Co^{2+} have been found in some spinels such as $CoRh_2O_4$.[21] The negative θ values for $Li_2CoTi_3O_8$ and $Li_2CoGe_3O_8$ are thus ascribable to weak, negative A–A interactions between Co^{2+}.

Electrical properties

In the ideal normal spinel structure $A[B_2]X_4$, space group *Fd3m*, each 8a tetrahedron occupied by A-cations shares common faces with four neighbouring empty 16c octahedra. A-cations can, therefore, move three-dimensionally through the possible diffusion pathway, 8a→16c→8a→16c→. For structures with $Y=0$, *i.e.*, $Li_2NiGe_3O_8$, only Li^+ ions occupy the 8a/16c sites. For $Y>0$, however, M^{2+} ions partially occupy the 8a sites and these may act to block the pathways for Li^+ ion conduction. For all *Y*, the cubic close-packed nature of anions in the spinel structure with full occupancy makes anionic conduction through spinel lattices unlikely.

Impedance data for $Li_2NiGe_3O_8$ at 243 °C are shown in Fig. 5. Two partly resolved arcs and a well formed spike are seen. The high frequency arc has an associated capacitance, calculated from the relation $\omega RC=1$ at the arc maximum of 7.9×10^{-12} F. This value is typical of the bulk (intragranular) response of the sample. The low frequency arc, with an associated capacitance of 1.2×10^{-10} F corresponds to a grain boundary (intergranular) resistance. The spike at low frequencies is inclined at *ca.* 30° to the horizontal axis, with an associated capacitance of $\approx6\times10^{-6}$ F, and is characteristic of electrode–electrolyte interfacial phenomena associated with partial or complete ion blocking and either a rough interface or Warburg diffusion. Similar, inclined spikes (not shown), at angles of 30–40° to the horizontal were also observed for $Li_2MgTi_3O_8$, $Li_2CoTi_3O_8$ and $Li_2CoGe_3O_8$: their associated capacitances were *ca.* 10^{-6}, 10^{-2} and 10^{-2}–10^{-3} F, respectively. Such high capacitance values for the latter two must be caused by ionic conduction together with significant amounts of electrochemical discharge at the metal electrodes.[23] For $Li_2ZnGe_3O_8$, the impedance response (not shown) was scattered at low frequencies in the measured temperature range 562–838 °C, Table 9; a poorly developed spike probably associated with ion blocking at the sample–electrode interface was, however, recognisable at high temperatures, *e.g.* 838 °C. In conclusion, the conductivities in the measured (high) temperature ranges appear to be dominated by Li^+ conduction for the spinels studied here; the conductivity of $Li_2ZnGe_3O_8$ is, however, extremely low, and the nature of the conducting species is not certain. The absence of measurable electronic conduction is further evidence for the absence of mixed-valence states for M and M′, as proposed in the magnetic results section.

Bulk conductivity data were extracted from the complex impedance plots, and are shown in Fig. 6 as a function of temperature. The conductivities, σ, fit the Arrhenius equation, $\sigma T=\sigma_0\exp(-\Delta H/kT)$, where σ_0 is the pre-exponential factor, and *k* Boltzmann's constant. The activation energies, ΔH, are characteristic of moderate to poor ionic conductors, Table 9. Because the structures are based on cubic close packing of oxygens, the bottleneck size for Li^+ hopping through the tetrahedral site-empty octahedral site conduction pathway proposed above is small, leading to the high observed activation energies. $Li_2ZnGe_3O_8$ possesses by far the highest ΔH (2.14 eV) of all the spinels studied here, and its conductivity is extremely low. Li^+ conduction through the pathway would be blocked significantly by Zn^{2+} located in tetrahedral sites for $Li_2ZnGe_3O_8$, $Y=0.5$. It may be seen that ΔH decreases with

Table 9 Conductivity Arrhenius parameters for spinel phases $Li_2MM'_3O_8$

composition	ΔH/eV	$\log_{10}$ (σ_0/S cm^{-1})	measured temperature range/°C
$Li_2ZnGe_3O_8$	2.14	8.08	562–838
$Li_2MgTi_3O_8$	0.71	3.99	163–440
$Li_2CoTi_3O_8$	1.33	6.94	349–640
$Li_2CoGe_3O_8$	1.49	6.86	440–638
$Li_2NiGe_3O_8$	0.55	3.46	63–268

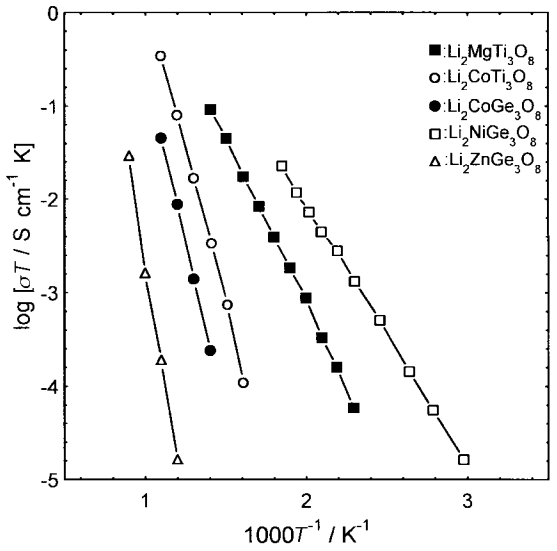

Fig. 6 Conductivity Arrhenius plots for spinel phases $Li_2MM'_3O_8$

decreasing Y, reaching 0.55 eV for $Li_2NiGe_3O_8$, $Y=0$, which has perfectly connected three-dimensional conduction pathways without any channel blocking agents in tetrahedral sites; further studies on possible correlations between ΔH and Y are in progress.

Electrochemical properties

Insertion/extraction of Li into/from $Li_2M^{2+}M'^{4+}{}_3O_8$ requires three-steps: (i) Li^+ migration into/out of $Li_2M^{2+}M'^{4+}{}_3O_8$; (ii), redox reactions for either M^{2+} or M^{4+} and (iii) electron/hole migration from/to the counter electrode to maintain charge neutrality. For all the spinels prepared in this work, step (i), *i.e.*, Li^+ migration is possible through the tetrahedral site-empty octahedral site pathway proposed above, although for $Y>0$, partial occupancy of tetrahedral sites by M may act as channel blocking agents.

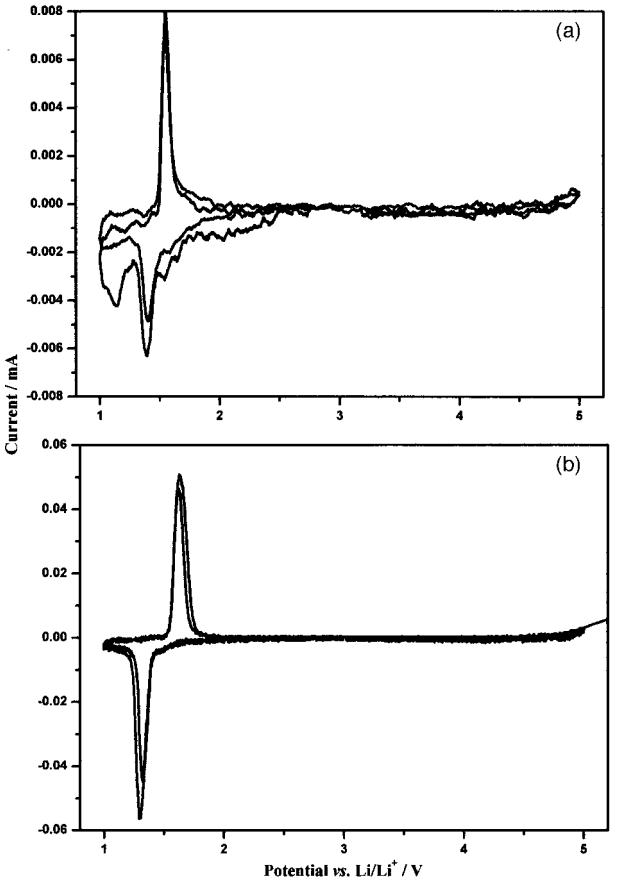

Fig. 7 Cyclic voltammograms for (a) $Li_2MgTi_3O_8$ and (b) $Li_2CoTi_3O_8$

Cyclic voltammograms show a set of reversible peaks at *ca.* 1.5 V *vs.* Li/Li^+ for the two titanates. The rest potential was *ca.* 3.5 V, and therefore the peaks in the cyclic voltammograms correspond to insertion/deinsertion of Li, Fig. 7. Redox reactions $M^{2+}+e \rightleftharpoons M^+$ are unlikely to take place, especially for M = Mg, Fig. 7, since the monovalent state is thermodynamically unstable for the M species. Lithium insertion/deinsertion appears, therefore, to be possible, but to be linked to the reaction, $Ti^{4+}+e \rightleftharpoons Ti^{3+}$. There were no detectable peaks on cyclic voltammograms for the germanates, consistent with the expectation that, unlike Ti^{4+}, Ge^{4+} is not readily reduced. Li insertion is thus prevented by the absence of step (ii) for the germanates.

Attempts to extract Li electrochemically from either titanates or germanates up to 5 V *vs.* Li/Li^+ were unsuccessful: no peaks were observed between *ca.* 3.5 and 5.0 V in the cyclic voltammograms. Among the spinels studied here, oxidation of Co^{2+} and Ni^{2+} is certainly feasible and Li has been extracted electrochemically from the spinel $Li_2NiMn_3O_8$, involving the oxidation reaction $Ni^{2+} \rightarrow Ni^{4+}+2e$.[24] In that case, electrons produced by the oxidation probably migrate through octahedral interstices occupied by Ni and Mn. For the titanates and the germanates studied here, octahedral 12d sites containing $Ti^{4+}(d^0)$ or $Ge^{4+}(d^{10})$ completely surround each octahedral 4b site containing M^{2+}. Even though electrons were produced by oxidation of M^{2+}, the succeeding electronic migration through octahedra would be blocked by the 12d octahedra occupied by Ti^{4+} or Ge^{4+}. Long-range electronic migration from octahedral M sites to tetrahedral M sites or *vice versa* would be difficult, because of very small (or no) concentration of M in either tetrahedral or octahedral sites. Moreover, the relatively long distances between tetrahedra would render electronic conduction through tetrahedral M sites unlikely. It is concluded that, although step (i) may be difficult to attain in the above samples, owing to the insulating behaviour at room temperature, Fig. 6, Li extraction could be prevented by the lack of long-range electronic conduction and the difficulty of step (iii) for the titanates and the germanates, including those with M = Co or Ni.

H. K. thanks CVCP for an ORS Award. We acknowledge the assistance of J. M. S. Skakle (Rietveld refinement of powder neutron diffraction data) and R. A. Howie (bond length calculations).

References

1 E. J. W. Verwey and E. L. Heilmann, *J. Chem. Phys.*, 1947, **15**, 174.
2 D. S. McClure, *J. Phys. Chem. Solids*, 1957, **3**, 311.
3 J. D. Dunitz and L. E. Orgel, *J. Phys. Chem. Solids*, 1957, **3**, 318.
4 A. Navrotsky and O. J. Kleppa, *J. Inorg. Nucl. Chem.*, 1967, **29**, 2701.
5 A. Durif and J. C. Joubert, *Compt. Rend.*, 1962, **255**, 2471.
6 G. Blasse, *J. Inorg. Nucl. Chem.*, 1963, **25**, 743.
7 J. C. Joubert and A. Durif, *Bull. Soc. Fr. Mineral Crist.*, 1963, **86**, 92.
8 J. C. Joubert and A. Durif, *Compt. Rend.*, 1963, **256**, 4403.
9 G. Blasse, *Philips Res. Rep. Suppl.*, 1964, **3**, 1.
10 G. Blasse, *J. Inorg. Nucl. Chem.*, 1964, **26**, 1473.
11 J. C. Joubert and A. Durif, *Compt. Rend.*, 1964, **258**, 4482.
12 G. Blasse, *Philips Res. Rep.*, 1965, **20**, 528.
13 V. S. Hernandez, L. M. T. Martinez, G. C. Mather and A. R. West, *J. Mater. Chem.*, 1996, **6**, 1533.
14 I. M. Hodge, M. D. Ingram and A. R. West, *J. Electroanal. Chem.*, 1976, **74**, 125.
15 R. D. Shannon, *Acta Crystallogr., Sect. A*, 1976, **32**, 751.
16 K. Hirota, M. Ohtani, N. Mochida and A. Ohtsuka, *J. Ceram. Soc. Jpn.*, 1988, **96**, 92.

17 T. Saito, N. Mochida and A. Ohtsuka, *Yogyo-Kyokai-Shi*, 1987, **95**, 604.
18 H. M. Rietveld, *J. Appl. Crystallogr*., 1969, **2**, 65.
19 H. Kawai and A. R. West, unpublished data.
20 R. C. Evans, *An Introduction to Crystal Chemistry*, Cambridge University Press, London, New York, 1964.
21 G. Blasse and D. J. Schipper, *Phys. Lett*., 1963, **5**, 300.
22 G. Blasse and J. F. Fast, *Philips Res. Rep*., 1963, **18**, 393.
23 H. H. Sumathipala, M. A. K. L. Dissanayake and A. R. West, *J. Electrochem. Soc*., 1995, **142**, 2138.
24 Q. Zhong, A. Bonakdarpour, M. Zhang, Y. Gao and J. R. Dahn, *J. Electrochem. Soc*., 1997, **144**, 205.

Paper 8/00234G; *Received* 7*th January*, 1998